Miniaturized dynamic light scattering instrumentation for use in microfluidic applications

Thomas Q. Chastek, Kathryn L. Beers,[a] and Eric J. Amis
Polymers Division, National Institute of Standards and Technology, 100 Bureau Drive Gaithersburg, Maryland 20899-8542

(Received 3 November 2006; accepted 22 January 2007; published online 10 July 2007)

Five designs for a miniaturized dynamic light scattering (DLS) instrument are described that incorporate microfluidic flow of the sample volume and fiber optic probes directly embedded into the sample. These instruments were demonstrated to accurately determine the size of 10–100 nm particles dispersed in organic and aqueous solvents with most sample sizes less than 150 μl. Small stir bars were incorporated directly into the instruments, and enabled blending of different solutions immediately prior to DLS measurements. Demonstration of the instruments' capabilities include high throughput measurements of the micelle to unimer transition for poly(styrene-*b*-isoprene) in mixed toluene/hexadecane solvent, obtained by systematically blending toluene-rich and hexadecane-rich polymer solutions. The critical solvent composition was quickly identified with less than 20 mg of polymer. Further capabilities include temperature control, demonstrated by identification of a critical micelle temperature of poly(ethylene oxide-*b*-propylene oxide-*b*-ethylene oxide), as well as multiangle DLS measurements. © *2007 American Institute of Physics.*
[DOI: 10.1063/1.2755569]

I. INTRODUCTION

Dynamic light scattering (DLS) is a powerful tool for characterizing, among other things, the size of particles as small as a few nanometers.[1] It is a relatively low cost technique that can be incorporated into a wide range of instrumentation with the use of fiber optic probes. For example, miniaturized DLS instruments have been designed to send into space,[2] been incorporated into high-pressure cells for measuring polymer dissolved in super critical carbon dioxide,[3] and been used for *in vivo* characterization of the vitreous fluid in a human eye.[4] While DLS instrumentation has been developing for decades, the concept of microfluidic measurement systems has begun to receive attention more recently.[5–7] A central focus in the area of microfluidics is the development of microscale total analysis systems (μTAS) or labs on a chip (LOC).[8] Dynamic light scattering is ideally suited for incorporation into microfluidic devices because it can be adapted to measure very small fluid samples. Furthermore, its ability to measure nanoparticle sizes and diffusion coefficients can make it a very useful component of many microfluidic systems. In the present work, microfluidic measurements are useful because they allow for high throughput characterization.

The use of microfluidic devices enables vastly reduced sample volumes, precise manipulation of the flow environment, and the potential for rapid sequential or parallel measurements. Many measurement tools have been applied to characterize fluids in microfluidic devices. The most common rely on some form of imaging, including optical, IR, fluorescence, and Raman microscopes. With the growing interest in nanosized structures, it is important to overcome current limitations in microfluidics for resolving and quantitatively measuring nanoparticles. Also, the physical size of the microscopes can limit the availability of precious space on the chips for integration of multiple measurements on the same device. Kuyper *et al.* have demonstrated the application of a confocal microscopy technique for quantitative nanoparticle sizing.[9] However, it is appealing to implement scattering techniques on a chip to obtain quantitative information regarding nanoparticle size and size distribution because scattering is routinely used with success to obtain this information in conventional sample volumes. Some examples of small angle light scattering[10] and x-ray scattering[11] have demonstrated this by mounting a chip in the path of a traditional macroscale instrument. Further reduction in infrastructure, accomplished in this work with the use of fiber optics, reduces the footprint of the measurement and increases the signal to noise ratio by minimizing optical problems such as refraction that arise when characterizing small samples through glass interfaces.

DLS instruments that made use of fiber optic probes were originally developed by Brown *et al.*[12] and Dhadwal and Chu.[13] In the development of this category of instrument, there was significant experimental[13–15] and theoretical[16] interest in evaluating the proper type of optical fibers to use: single or multimode. Dhadwal and Chu argued, based on their experiments, that multimode fibers are better because they accept the most light. They found this to improve the ability to collect sufficient signal on a reasonable time scale. The general consensus of other groups was that single mode fibers are better because their low numerical aperture defines a small coherence volume, which improves

[a]Author to whom correspondence should be addressed; FAX: 1-301-975-4924 electronic mail: Kathryn.Beers@nist.gov

the data quality. The fiber optic DLS instruments that have been constructed possess several advantages. For example, Egelhaaf and Schurtenberger used fiber optic probes to simplify the detector optics, alignment, and overall design of a multiangle DLS/static light scattering instrument.[17] Brown used the fiber optic probes to design a homodyne DLS instrument.[18] Fiber optic connections simplified the splitting and mixing of signals. Most of the instruments that were constructed, however, placed the probes outside a transparent sample cell, but an article by Dhadwal and Chu discussed the potential advantages of bringing the probe in direct contact with the sample.[13] They demonstrated this with the construction of a high pressure cell.[3] Their instrument allowed observation of the self-assembly of fluoropolymers in supercritical carbon dioxide.

In this article we describe the construction of several DLS instruments with flow-through microfluidic designs. All of the designs had fiber optic probes embedded directly into the sample. This permitted the sample volumes to be miniaturized and high throughput measurements to be made with sufficiently little sample consumption. The ability of the instruments to accurately determine the size of nanoparticles was evaluated by measuring latex spheres and block copolymer micelles. Incorporation of a stirring element allowed solutions to be blended together immediately prior to DLS measurements. This provides the means for systematic high throughput measurement of a combinatorial library, for example, by mixing together ratios of two or more stock solutions. High throughput measurements were demonstrated by blending solutions of poly(styrene-*b*-isoprene) in different solvents to determine the critical solvent composition for micelle formation. Furthermore, the temperature control ability of some devices were demonstrated by measuring the critical micelle temperature (CMT) of an aqueous solution of a poly(ethylene oxide-*b*-propylene oxide-*b*-ethylene oxide) (trade name Pluronic). In addition, strategies for extending these designs to include multiangle measurements are presented and evaluated.

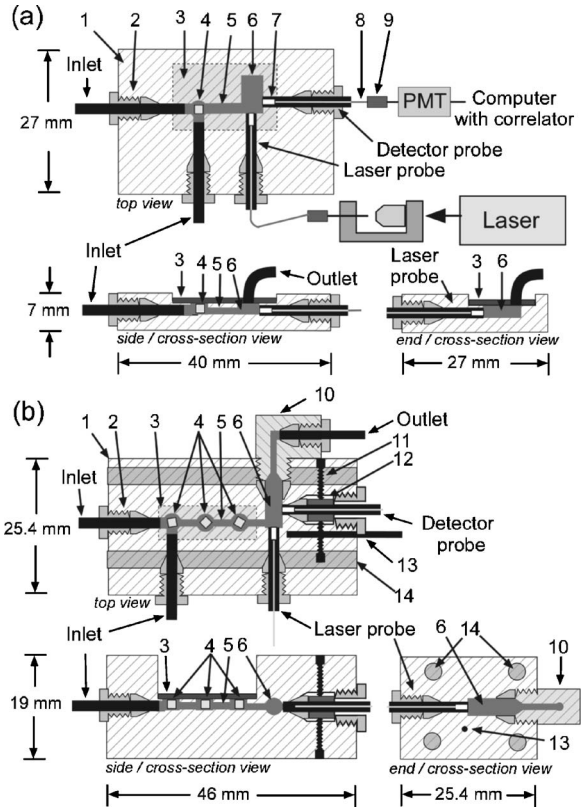

FIG. 1. Diagrams of devices 1a and 1b. Everything is drawn to scale, except for the PMT, laser, and focusing lens assembly. Device 1a is a simplified single angle instrument. Two inlets with Teflon tubing inserted (o.d.=1.6 mm, i.d.=0.8 mm) to introduce solutions to mixing and measurement chambers before exiting the top. Laser light is sent into the sample and scattered light is collected through fiber optic probes (o.d.=1.6 mm). Device 1b includes additional features, such as a fully enclosed measurement chamber, adjustable detector probe, and heating cartridges. Further details of these devices are listed: (1) aluminum housing anodized black, (2) stainless steel HPLC nut with Teflon ferrule, (3) glass or aluminum cover, (4) mixing chamber/s (ϕ=3.2 mm, depth=2 mm) with magnetic stir bar (ϕ=1.6 mm, L=1.6 mm), (5) internal channel (ϕ=1.0 mm), (6) measurement chamber (device 1a: $7\times4\times3$ mm^3; device 1b: ϕ=3.2 mm, L=9 mm), (7) GRIN microlens (ϕ=1.0 mm, L=2.3 mm), (8) polarization maintaining single mode optical fiber, (9) FC/PC fittings and coupler, (10) aluminum elbow, (11) one of four set screws for alignment, (12) collar for detector probe, (13) thermocouple (ϕ=1 mm), and (14) heating cartridge (ϕ=3.2 mm, L=51 mm).

II. INSTRUMENTATION[19]

A series of five instruments were made and are shown in Figs. 1 and 2 and described in Table I. An important aspect of these devices is the fiber optic probes, which were based on the work of Dhadwal and Chu.[13] A single standard type of probe was used in all instruments, and is depicted in Fig. 3. They were made from stainless steel high performance liquid chromatography (HPLC) tubing [outside diameter (o.d.) =1.59 mm, inside diameter (i.d.)=254 μm]. A 1.0 mm hole was drilled into one end of the tube (diameter=1.0 mm, length z=2.3 mm) to accept a 1.0 mm diameter 0.23 pitch gradient refractive index (GRIN) lens, purchased from NSG America. The index gradient constant, $\sqrt{A}$, was 0.62 mm^{-1}, and the core refractive index, N_o, was 1.62. The lens was secured in place with epoxy. A single-mode polarization-maintaining optical fiber that was suited for λ=488 nm (Fibercore HB450 from Thorlabs) was polished and inserted into the 254 μm hole of the HPLC tubing. The fiber had a numerical aperture of 0.115 and a core diameter, D_f, of 3.6 μm. The fiber was aligned in the probe by evaluating the quality of collimation of laser light sent through the probe. Once aligned, the fiber was epoxied to the HPLC tubing. Using the lens and fiber parameters, the angular uncertainty, $(\Delta\theta)_f$, and effective pupil entrance, D_A, can be calculated from equations presented in Appendix A of Ref 13. The probes used in this work had $(\Delta\theta)_f$=1.4 mrad and D_A=230 μm, and this is shown in Fig. 3. The fiber exiting the probe was fitted with a fiber coupling (FC/PC) connector for simplicity in connecting the probe to the laser or photomultiplier tube (PMT). This allowed a single type of probe to be used in the laser and detectors of all the instruments.

The laser light (50–300 mW beam from an Ar ion laser, λ=488 nm, Lexel 75)[19] was launched into a fiber using a Newport fiber coupler (model F1015)[19] with a 20× microscope objective. Some measurements required increased in-

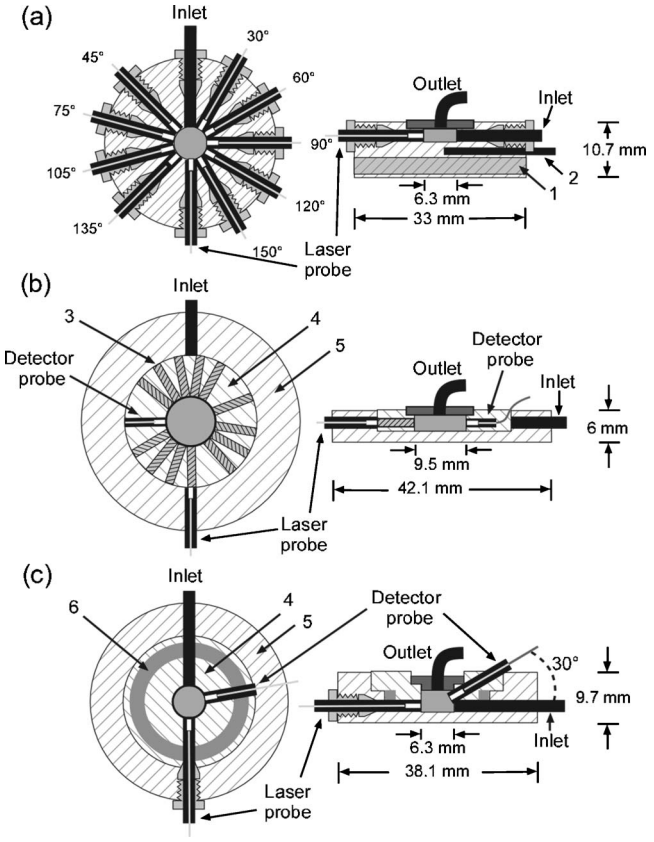

FIG. 2. Diagrams of devices 2a–2c are drawn to scale, with the left-hand column depicting the top view and the right-hand column depicting a cross-sectional side view. These three multiangle devices have measurement chambers located at their center (device 2a: ϕ=6.3 mm, d=2 mm; device 2b: ϕ=9.5 mm, d=3 mm; device 2c: ϕ=6.3 mm, d=4 mm) and have outlets attached to their covers. Device 2a has detector probes located at nine fixed angles. Device 2b has a short detector probe that rotates within the stationary base. Device 2c has a rotating detector probe aligned 60° to its axis of rotation. Further details of these devices are listed: (1) heating cartridge (ϕ=3.2 mm, L=51 mm), (2) thermocouple (ϕ=1 mm), (3) one of 13 open channels to allow the laser light to reach the sample as the detector probe is rotated (ϕ=1.6 mm, L=7 mm), (4) rotating ring that contains the detector probe (in devices 2b and 2c, ϕ=25.4 mm) (5) stationary cup-shaped base with laser probe, and (6) Teflon o ring (o.d.=20 mm, i.d.=16 mm).

tensity. This was done by (1) increasing the intensity of the laser, (2) further polishing the fiber that accepted the laser light, and (3) replacing the 20× objective with a 50× objective. Strategies (2) and (3) are more relevant when using a low intensity laser (e.g., a helium-neon source). Visual observation of the laser beam leaving the probe determined that

TABLE I. Instrumental characteristics.

	Total internal volume (μl)	Available angles	β value[a]
Device 1a	111	90	0.92±0.04
Device 1b	153	90	0.97±0.01
Device 2a	65	30–150[b]	0.92±0.03
Device 2b	213	10–150[c]	0.95±0.01
Device 2c	125	30–150	0.96±0.04

[a]Uncertainty is the standard deviation in the data set.
[b]Nine angles in 15° increments.
[c]13 angles in 10° increments.

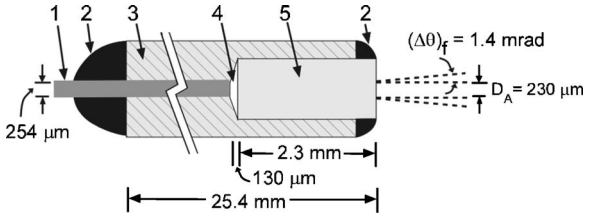

FIG. 3. Optical geometry of the fiber optic probes. The probe is drawn to scale with the exception of the length, as is indicated by the break. The effective pupil, D_A, and angular uncertainty, $(\Delta\theta)_f$, were calculated from equations in Appendix A in Ref. 13. Aspects of the probe include (1) polarization maintaining single mode fiber with numerical aperture of 0.115 and core diameter of 3.6 μm, (2) epoxy to seal the fiber and lens in place, (3) stainless steel tube (o.d.=1.6 mm, i.d.=254 μm), (4) air gap which is required because the lens has a 0.23 pitch that places the focal point off the back surface of the lens, and (5) GRIN microlens (ϕ=1.0 mm, L=2.3 mm).

it was approximately 200 μm in diameter with a divergence angle of approximately 3 mrad, which agrees with the calculated values of $(\Delta\theta)_f$ and D_A. The detector probes were connected to a PMT (Hamamatsu HC120-08).[19] The PMT was tightly wrapped in black plastic and the room lights turned off to reduce stray light from reaching the detector. The signal was converted to a digital transistor-transistor logic (TTL) format and sent to a BI9000AT correlator (Brookhaven Instrument Corp.).[19] The fibers from the PMT, laser, and probes were all terminated in FC/PC connectors, and this allowed for devices to be easily swapped.

Device 1a, shown in Fig. 1(a), has a single detection probe at 90°. The device housing was machined from aluminum and anodized black to reduce reflections. Samples were introduced with computer controlled syringe pumps though Teflon tubing (o.d.=1.59 mm, i.d.=0.79 mm), which was connected to the aluminum housing with HPLC fittings consisting of stainless steel nuts and Teflon ferrules. The probes were also attached with these fittings, which were found to both simplify assembly of the device and successfully eliminate leaks. In device 1a, the two inlets meet at a mixing chamber. This aspect of the design allows for microliter quantities of two different solutions to be mixed immediately prior to measurements. Thus, a series of various compositions can be measured in a high throughput manner. A neodymium magnet (diameter=1.59 mm, L=1.59 mm, K&J Magnetics, Inc.)[19] is used as a miniature stir bar. Both the mixing and measurement chambers were milled from the top down and a piece of glass was secured to the top with high temperature silicone glue. The outlet of the devices was inserted into a hole drilled through the top. The outlet tube was positioned this way to help prevent bubbles from being trapped in the measurement chamber. This was a more significant issue for aqueous systems, which tended to preferentially wet the aluminum oxide surface instead of glass. The measurement chamber was 7×4×3 mm, and the laser beam was directed down the length of the channel to minimize its contribution to the detected light. Device 1a had a 13 μl mixing cavity after excluding the magnet volume and an 84 μl measurement chamber. It should be noted that the measurement chamber was somewhat large by microfluidic standards because of concerns that light reflected or scattered off the walls might distort the results by mixing with the scattered

signal at smaller dimensions. Because this problem was not observed in any of the devices that were made, it is expected that significant reductions in device dimension will be straightforward.

In this work, the scattering angle, θ, was determined by observation prior to data collection. In most cases, θ directly resulted from how the devices were machined, which resulted in very little uncertainty $<\pm 0.5°$. While it is generally valid to use size standards to assist in the determination of θ, this was avoided because the size standards were used to evaluate the accuracy of the devices.

Table I describes some characteristics of the devices, such as the total internal volume, available angles, and coherence factors β. The β value is a measure of the beating efficiency, ranges from 0 to 1, and depends on the ability of the instrument to effectively detect the scattered light. In our work, we extracted β values from the amplitude of the quadratic cumulant fits. Table I lists the average β values associated with each device for all the data presented in this paper. The standard deviation is shown to indicate the spread in the data. Device 1a, and all of the others, consistently had very high β values that were mostly above 0.90, indicating that they had remarkably high signal to noise ratios.

Device 1b, shown in Fig. 1(b), includes a few added features not present in the original simplified design. Even though mixing in device 1a was found to be sufficient, three mixing chambers were included to allow for sufficient mixing at faster flow rates. It was determined that the magnets needed to be a minimum of 6 mm apart so that their magnetic fields did not interfere with their rotation. Also, the exit tube was connected to an elbow made of black anodized aluminum. This eliminated the glass top, which brought four benefits: (1) Reflections off the glass surface were reduced. (2) There was no longer a problem of getting aqueous solutions to wet the glass. (3) The new design acted as a better light trap for the laser beam. (4) Heating cartridges could be placed above and below the sample to provide more uniform heating. The issue of uniform heating is important in DLS because thermal gradients lead to convection and prevent the accurate determination of diffusion coefficients. The device incorporated four heating cartridges (diameter=3.18 mm, L=50.8 mm, Watlow Firerod) and a thermocouple connected to a temperature controller (Omega CN77600) run by a LABVIEW program.[19] The final improvement in this device was a means of fine tuning the detector probe orientation. The detector probe was inserted into an oversized hole with the tip securely centered with the Teflon ferrule. Four setscrews could be adjusted to move the shaft of the probe within the hole until it was oriented such that lines of sight of the laser and detector probes perfectly intersected. It was found that this method of alignment significantly increased the detected intensity and improved the data quality.

The instrumental concepts described in Fig. 1 were applied to multiangle DLS measurements by the design of three additional devices, shown in Fig. 2 (devices 2a, 2b, and 2c, respectively). Under ideal situations, the angular dependence of DLS data should be well known, thus making data from only a single angle necessary. However, there are often cases when data from a single angle are of questionable reliability.

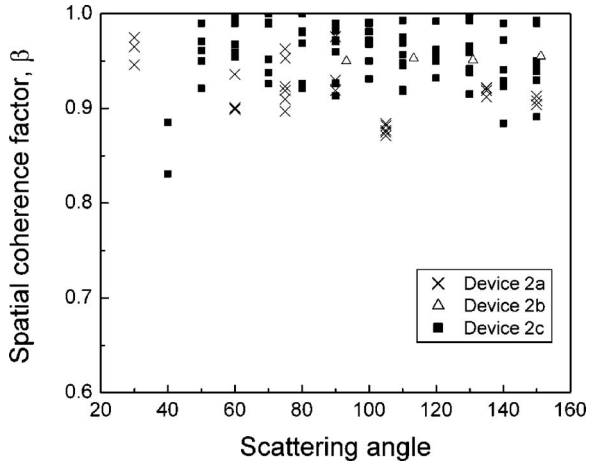

FIG. 4. Coherence factors, β, for the multiangle devices. The values were obtained from the amplitude of the quadratic cumulant fits.

This sometimes occurs with samples that scatter too weakly or are too concentrated. Measurements of multiple angles provide more data to determine how accurate the observed values are. Moreover, multiangle measurements are important for using the devices for static light scattering, but this will not be discussed in this article.

A device that had detector probes mounted at nine fixed angles is shown in Fig. 2(a). The angles range from 30° to 150° at 15° increments. The probes are 1.59 mm in diameter and in direct contact with the solution, limiting how much the circumference of the measurement chamber can be reduced. With ten probes and an inlet tube, it was found that a measurement chamber of 6.35 mm diameter and 2 mm depth was sufficiently large. This gave a measurement chamber volume of 65 μl. The sample chamber was sealed with a glass disk, and an outlet tube was attached to a hole drilled in the glass cover. On occasions where temperature stability was needed, the glass cover was replaced with an anodized aluminum one. Glass was used in the early testing phase to enable visual confirmation that no bubbles were present. The β values for this and the other multiangle devices were quite high and did not have any remarkable angular dependence, as is shown in Fig. 4.

The design of device 2a is similar to previously designed multiangle devices. For example, the instruments designed by Egelhaaf and Schurtenberger[17] and Bantchev *et al.*[20] consisted of aligning several detector probes around a transparent sample cell. Zhou *et al.*[3] embedded the probes into the sample. Putting the probes directly in contact with the samples eliminated the need to hold the sample in glass cells, and we found this to have several advantages: (1) Refraction from curved glass surfaces was avoided. This typically is an increasingly likely problem as the sample volume decreases. (2) The thermal stability was improved. (3) It generally simplified constructing, aligning, and cleaning the devices.

The use of multiple detector probes brings with it the question of where to direct the signals. In our device, we manually switched probes connected to the PMT, but various automated strategies have been developed. Bantchev *et al.* connected a PMT to each detector probe and either four or eight of the PMTs were connected to a multichannel cor-

relator card.[20] Engelhaaf and Schurtenberger also used multiple PMTs, but used digital multiplexers to select which signal reached a single correlator.[17] Zhou *et al.* described a method for selecting a single signal from multiple fibers by aligning them radially, focused on a central point.[3] A mirror aligned at 45° to the fibers was rotated at the point, and selectively directed only one of the signals down to a PMT. Finally, Haller *et al.* used solenoid operated shutters to block all signals except the one of interest from reaching a single PMT.[21]

Another strategy for multiangle measurements is to rotate a single detector probe. When the sample is contained in a transparent cell and no refractive index matching fluid is used, the probe can be freely moved about without restrictions. In this work, however, we desire to have the laser and detector probes embedded directly into the sample. This brings restrictions because the nontransparent housing must contain the liquid samples and allow both probes unimpeded contact with the sample at several angles. Figure 2(b) shows a device that addresses this restriction by using a very short detector probe. The probe is inserted into a ring that is rotated with respect to the shallow cup-shaped base it is placed in. The laser probe is inserted into the base. Several additional channels were drilled into the ring to allow the laser light to pass into the sample. In all, 13 channels were made, to allow for measurements at angles ranging from 10° to 150°.

Figure 2(c) shows another approach to having a rotating detector probe. In this case, the detector probe was no longer perpendicular to the rotation axis, instead it was offset by 60°, as depicted in the Fig. 2(c). The laser probe was perpendicular to the axis of rotation. When the detector was rotated to its minimum angle (directly opposite of the laser probe) the scattering angle, θ, was 30°, and when the detector was directly above the laser probe, θ was at its maximum of 150°. The relationship between the angle of rotation, α, and the scattering angle, θ, is $\cos\theta = \sqrt{3}/2 \cos\alpha$. Because the detector probe was above the laser probe it could be freely rotated, which allowed for measurement at any angle between $30° < \theta < 150°$. As was the case with device 2b, there is a tube connected opposite to the laser probe, which acts as a sample inlet and as a light trap. The outlet is inserted into a hole drilled into the glass or aluminum top. In device 2c, a Teflon washer was used to improve the seal between the base and rotating ring. The measurement chamber for device 2b was 213 μl, but was reduced to 125 μl in device 2c.

The five devices that were described all consist of machined metal housing with fiber optic probes embedded directly into the sample. This design approach is extremely simple allowing for the production of devices for custom applications. In this case, devices were made to have microfluidic designs useful for making high throughput measurements. Also, devices were made to demonstrate this strategy can be extended to multiangle instruments.

III. EXPERIMENT

To demonstrate our devices, measurements were made on solutions of latex polystyrene nanoparticles and block copolymers. The nanoparticles that were used had diameters listed at 64 nm±2.8 nm (Duke Scientific, 1% solids, mass fraction) and 107.6 nm (Polysciences, Inc., Polybead polystyrene microspheres 2.6% solids by mass with a coefficient of variance=15%).[19] Latex solutions were diluted with deionized water until the solution was only slightly cloudy (approximately 0.001% solids by mass). Additionally, four block copolymers were used. One of them was Pluronic P85 (BASF lot WPDR-516B) which is poly(ethylene oxide-*b*-propylene oxide-*b*-ethylene oxide) (PEO-PPO-PEO). The PEO and PPO blocks had number average molecular masses of 1100 and 2300 g/mol, respectively. The other three block copolymers, purchased from Polymer Source, consist of a poly(styrene-*b*-isoprene) (PS-PI) and two poly(styrene-*b*-butadiene)s (PS-PB). The PS-PI had block number average molecular masses of 11 500 and 10 500 g/mol, respectively, and is denoted SI(11-10). The first PS-PB had block number average molecular masses of 5400 and 5350 g/mol, respectively, and is denoted SB(5-5). The other PS-PB had block number average molecular masses of 9400 and 9000 g/mol, respectively, and is denoted SB(9-9). Both the isoprene and butadiene block consisted of 1-4 addition, and had polydispersity indices of 1.03–1.04. The SI and SB copolymers were dispersed in hexadecane at concentrations of 2% volume fraction by using methylene chloride as a cosolvent. The solutions were placed under a gentle flow of nitrogen until the methylene chloride was removed (about 2 days). For solutions with mixed hexadecane and toluene solvents, the polymer was first dispersed in hexadecane to give a final volume fraction of polymer (ϕ_{polymer})=0.02 after the addition of toluene. All of the solutions were filtered with 0.2 μm filters prior to measurements in order to remove any dust.

The samples were introduced into the devices with computer controlled syringe pumps (Braintree Scientific, Inc., BS-8000).[19] The solutions were loaded into 5 ml plastic syringes and pumped at flow rates of 10–100 μl/min. The flow was stopped around 5 s prior to the start of data collection, which typically lasted 60 s, but occasionally took as long as 20 min. The stirring element was also stopped during measurements to prevent turbulence, which affects the observed diffusion coefficient. The measurements of particle size and scattered intensity were typically repeated at least twice at each angle or temperature. Measurements of scattered intensity were collected for at least 3 min to reduce the random error introduced by a rare spike in intensity caused by a dust particle passing through the measurement volume. The collection time typically could have been reduced below 3 min without problem, to accelerate measurements. In every case, a temperature controller was used to maintain the desired temperature.

IV. RESULTS AND DISCUSSION

The application of this instrumentation for high throughput measurements was demonstrated by systematically characterizing small aliquots of a sample prepared with various solvent compositions. This strategy allowed the critical composition for micelle formation to be easily identified. Further

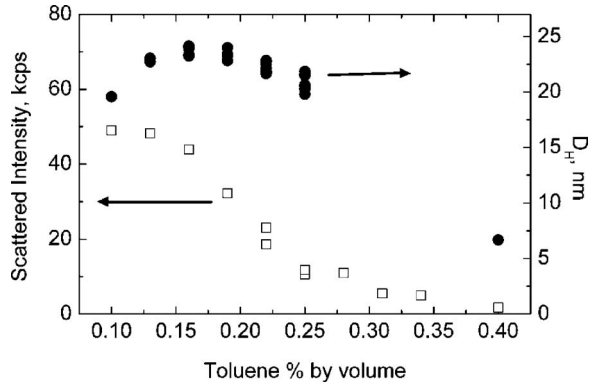

FIG. 5. Measurements of a series of poly(styrene-*b*-isoprene) solutions that have a mixed hexadecane/toluene solvent of varying composition. Above 25% by volume toluene, the micelles (D_H=22 nm±3 nm) dissociate into unimers ($D_H \cong 7$ nm). High throughput measurements allowed this critical composition to be rapidly identified with less than 20 mg of polymer.

measurements include a temperature scan to identify a CMT. In addition, the multiangle instrumental designs were evaluated and compared.

High throughput measurements were made by characterizing SI(11-10) in a mixed solvent of hexadecane and toluene. Toluene is a neutral solvent for polystyrene and polyisoprene, which results in poly(styrene-*b*-isoprene)s remaining in a unimer state. Hexadecane, on the other hand, is selective for the polyisoprene blocks. Thus, micelles form in hexadecane with polyisoprene coronas and polystyrene cores. When poly(styrene-*b*-isoprene) is dissolved in a mixed toluene/hexadecane solvent at room temperature, it may be in either a micelle or unimer state depending on the relative amounts of hexadecane and toluene. That is, a sufficiently hexadecane-rich solvent will induce micelle formation whereas a sufficiently toluene-rich solvent will not. Figure 5 shows data taken at 25 °C for solvent compositions ranging from 10% by volume to 40% by volume toluene. Both the particle size and scattered intensity were measured. Measurements were made in device 1a by blending together a toluene-rich solution [$\phi_{SI(11\text{-}10)}$=0.02, ϕ_{C16}=0.59, ϕ_{tol}=0.39] and a hexadecane-rich solution [$\phi_{SI(11\text{-}10)}$=0.02, ϕ_{C16}=0.88, ϕ_{tol}=0.10]. The two solutions were blended at flow rates totaling 100 μl/min for 110 s, resulting in 180 μl sample aliquots. The flow rates were relatively slow in order to provide the solution sufficient residence time in the mixing chamber. The aliquot volumes were sufficiently large to purge the entire device given that the mixing and measurement chambers had a combined volume of 100 μl. The sample flow and the mixing element were stopped prior to taking measurements because they affect the observed diffusion coefficient. Particle sizes were assigned with cumulant fits. More complex fits were unnecessary because the copolymer and associated micelles were nearly monodisperse. The requisite collection time increased as the scattered intensity decreased. For example, the hexadecane rich solution with ϕ_{tol}=0.10 scattered 50 kcounts/s (kcps), allowing for an accurate particle size to be determined in a few seconds. On the other hand, the toluene rich sample with ϕ_{tol}=0.39 scattered 1.7 kcps, requiring more than 20 min to measure the particle size. The viscosity of the mixed solvent was estimated by averaging the viscosities of the pure solvents (η_{C16}=3.03 cP, η_{tol}=0.56 cP) as in Eq. (1)[22],

$$\log(\eta) = \phi_{C16} \log_{(\eta_{C16})} + \phi_{tol} \log_{(\eta_{tol})}. \quad (1)$$

The refractive indexes of the blends were estimated by averaging those of the pure solvents (n_{C16}=1.50, n_{tol}=1.43) as shown in Eq. (2).

$$n = \phi_{C16} n_{C16} + \phi_{tol} n_{tol}. \quad (2)$$

The scattered intensity was determined after collecting signal for at least 3 min.

The data in Fig. 5 indicate that the critical solvent composition for micelle formation is 25% by volume toluene, 75% by volume hexadecane. The particle size data show that micelles with hydrodynamic diameters (D_H) of 19.5–23.9 nm are present until the solvent contains 25% by volume toluene. At higher toluene compositions, particle sizing became prohibitively difficult. The sudden difficulty in obtaining a smooth autocorrelation function occurs because the micelles are no longer present. At the transition point, the spread in the micelle size data increases because the scattered signal from the micelles is decreased. The polymer in the unimer state was measured at ϕ_{tol}=0.40 and found to have a D_H=6.7 nm. The scattered intensity is also a good measure of the transition because the micelles scatter more strongly than the unimers. Measuring the scattering intensity is easier than particle sizing, but the transition is not as clearly identifiable. The data show the scattered intensity steadily decreasing as the CMC is approached from the hexadecane rich side. The drop off in intensity stabilizes beyond the critical composition. Measurements of the particle size and scattered intensity, the transition from micelle to unimer can be accurately determined.

This type of high throughput measurement is expected to be applicable to a variety of situations. For example, one could examine nanoparticles in more complex solvent mixtures, which, for example, have an additional number of solvents, change *p*H, or include salts or other solutes. As a wider number of parameters are included in the analysis of the nanoparticles' properties, the preparation of individual samples becomes impractical. Added sample complexity could easily be accommodated in the devices by introducing additional inlets. Moreover, since this is designed as a microfluidic device, the sample could be flowed into a subsequent analysis position. That is, this DLS measurement strategy can be integrated into a more complex lab on a chip.

In addition to measuring various samples, a single sample can be examined at several temperatures. An example of these devices' temperature control capability is shown in Fig. 6. The polymer, Pluronic P85, is water soluble and forms micelles at elevated temperature. At lower temperatures micelles do not form because the enthalpic energy gained by micelle formation is insufficient to overcome the accompanying loss in entropy.[23] The data in Fig. 4 were collected on a single sample using device 2a, with θ=135°. The temperature was slowly cooled from 40 to 24 °C over the course of 45 min. A micelle size of D_H=14–15 nm was observed above 30 °C. The scattered intensity steadily decreased as the temperature was reduced until 29 °C. Below

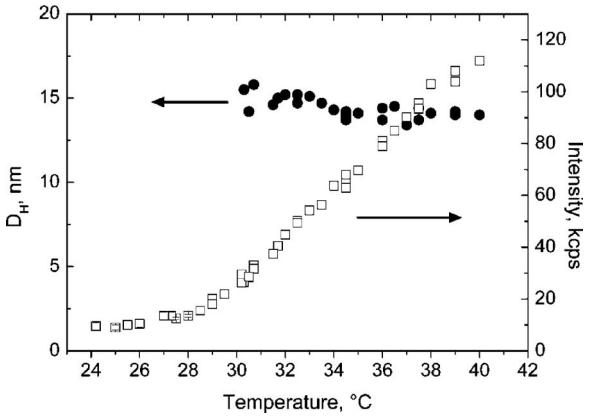

FIG. 6. Measurement of Pluronic P85 at 2% by volume in water. Micelles are present above the CMT, which is between 29 and 30 °C. The scattered intensity rapidly increases above the CMT.

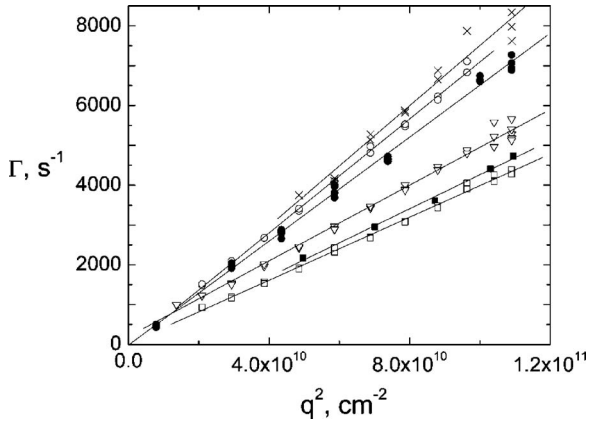

FIG. 7. Plotting Γ vs q^2 gives slopes equal to the diffusion coefficients. The values of D_H are calculated using the diffusion coefficients. Data were obtained from devices 2a–2c at angles ranging from 30° to 150°. The data are: (■) 107 nm latex measured with device 2b, (●) 64 nm latex measured with device 2a, (□) 107 nm latex measured with device 2c, (○) 64 nm latex measured with device 2c, (×) SI(5-5) measured with device 2c, (▽) SI(9-9) measured with device 2c.

this, the drop off in scattered intensity slowed. These results show the CMT for Pluronic P85 at 2% volume fraction in water to be 29–30 °C. This agrees with previous results obtained by Mortensen.[24]

The thermal properties of these devices are a key aspect of their design. The devices are capable of examining temperature dependent size phenomena, and they have the thermal uniformity to prevent convection. This is not the case for most microfluidic devices, such as polydimethylsiloxane chips. Additionally, it should be noted that these devices could also be cooled by circulating a chilled liquid through the housing. Condensation, which is a common problem of low temperature light scattering measurements, should not form because the glass/air interfaces were eliminated.

Figure 7 and Table II show data collected with the multiangle devices described in Fig. 2. The linewidth, Γ, values were obtained by fitting with a second moment cumulant fit. Plotting Γ versus the square of the scattering vector, q, gives a slope equal to the diffusion coefficient, D. The hydrodynamic diameter is obtained with the Stokes-Einstein relation shown in Eq. (3),

$$D = \frac{k_b T}{6\pi\eta(D_H/2)}. \tag{3}$$

In this equation, k_b is Boltzmann's constant and η is the solvent viscosity. The data in Fig. 7 were taken using devices 2a–2c at scattering angles of $30° < \theta < 150°$. It should be noted that the scattering angles were found by carefully determining the relative positions of the detector and laser probes prior to data collection. This method of determining the scattering angle had an uncertainty of around ±0.5°, which introduced some random error in the data, but should not systematically affect the slope. It should be emphasized that the scattering angles were not determined based on the scattering results.

The ability of these devices to provide accurate particle size information was tested by measuring monodisperse latex particle solutions. There was some limitation in using these standards because, as noted above, there was a small amount of uncertainty in their size as manufactured. Moreover, the process of diluting them could induce some aggregation. The particle sizes observed by the devices were typically within 5% of the manufacturers' determined average sizes. This agreement is quite good given that at least some of the discrepancy arose from the sample instead of the instrument. All of the DLS measurements were repeated multiple times, primarily to verify that the data were not skewed by a dust particle. Furthermore, several samples were measured with a Malvern Zetasizer 3000 HS for comparison. The Zetasizer 3000 measurements were repeated 20 times for each sample.[19,25]

Device 2a performed quite well, as was expected because similar fixed angle designs have been previously shown to work.[3,17,20] It provided a particle size to within 5 nm of the manufacturer's determined size. There was, however, difficulty in aligning the probes at 45° and 120° so data were not taken at those angles. Device 2b was much less

TABLE II. Particle sizes determined from data in Fig. 7.

	Device 2a		Device 2b		Device 2c		Commercial instrument
Sample	D_m, cm^2/s	D_H, nm	D_m, cm^2/s	D_H, nm	D_m, cm^2/s	D_H, nm	D_H, nm
Latex 64 nm	6.51×10^{-8}	69.1	···	···	7.16×10^{-8}	62.9	74.0
Latex 107 nm	···	···	4.28×10^{-8}	105	3.96×10^{-8}	114	112
SB(5-5)	···	···	···	···	7.51×10^{-8}	19.2	23.1
SB(9-9)	···	···	···	···	4.75×10^{-8}	30.3	33.0

of a success. It did collect accurate measurements, but it was prohibitively difficult to load the sample. Specifically, it was difficult to fill the channels in the rotating ring that allowed the laser light to reach the center. The aqueous latex solutions did not easily wet the channel walls, and instead leaked out of the device. Moreover, the somewhat larger size of the measurement chamber (diameter=9.5 mm) made alignment of the laser and the detector probes more challenging.

These limitations were addressed in device 2c by reducing the size of the measurement chamber (diameter=6.35 mm) and adding a Teflon *o* ring. The Teflon ring made a tight seal between the rotating top and the stationary bottom, preventing leaks. Thus, there were no problems with containing or flowing the sample. One unusual aspect of this device was that the detector probe was not perpendicular to its axis of rotation. As a result, the orientation of the light polarization changed as a function of scattering angle. Despite this, the spatial coherence values, β, were consistently high, as can be seen in Fig. 4. Moreover, the plots of Γ vs q^2 for four samples are shown in Fig. 7, and are quite accurate in describing the nanoparticle size. The measurement of the latex solutions were accurate to within 5% of the manufacturers' determined average sizes. In addition, the measured block copolymer micelle sizes are within 4 nm of those measured with the commercial instrument.

In general, the data in Fig. 7 demonstrates that the instrumental strategies used to make single angle high throughput DLS measurements can be extended to include multiple angles. Moreover, the data compared well to the measurements made with the Zetasizer 3000, which measured only at $\theta=90°$.

V. SUMMARY

Several DLS instruments were described and their capabilities were demonstrated. High throughput measurements were made on solutions of a poly(styrene-*b*-isoprene) in mixed toluene/hexadecane solvent. The critical solvent composition for micelle formation was identified by systematically blending together toluene-rich and hexadecane-rich solutions. The design of device 1a allowed for convenient solution blending, and required only 20 mg of polymer for a detailed identification of the critical composition. Identification of a thermally induced transition (i.e., CMT) was also demonstrated. A 2% by volume solution of Pluronic P85 in water was observed to have a CMT of 29 °C. Finally, three designs were presented for incorporating multiangle measurements, and found to provide accurate values. In general, this instrumentation is expected to allow for further high throughput measurements to be made on various complex nanoparticles solutions. Moreover, it can provide a route for incorporating DLS onto more complicated microfluidic labs on a chip.

ACKNOWLEDGMENTS

The authors thank Professor Dan Savin at the University of Vermont, Professor Tim Lodge and Will Edmonds at the University of Minnesota, and Dr. Anthony Bur at NIST for their helpful suggestions, and Dr. Thuy Chastek at NIST for help with the Zetasizer 3000 measurements. One of the authors (T.Q.C.) was supported by a NIST/National Research Council Postdoctoral Associateship. This work was carried out at the NIST Combinatorial Methods center (NCMC; www.nist.gov/combi).

[1] B. J. Berne and R. Pecora, *Dynamic Light Scattering* (Dover, Mineola, 2000).
[2] R. B. Rogers, W. V. Meyer, J. X. Zhu, P. M. Chaikin, W. B. Russel, M. Li, and W. B. Turner, Appl. Opt. **36**, 7493 (1997).
[3] S. Q. Zhou, B. Chu, and H. S. Dhadwal, Rev. Sci. Instrum. **69**, 1955 (1998).
[4] L. Rovati, F. Fankhauser, and J. Ricka, Rev. Sci. Instrum. **67**, 2615 (1996).
[5] E. J. Amis, Nat. Mater. **3**, 83 (2004).
[6] A. Manz, N. Graber, and H. M. Widmer, Sens. Actuators B **1**, 244 (1990).
[7] G. M. Whitesides, Nature (London) **442**, 368 (2006).
[8] D. Erickson and D. Q. Li, Anal. Chim. Acta **507**, 11 (2004).
[9] C. L. Kuyper, K. L. Budzinski, R. M. Lorenz, and D. T. Chiu, J. Am. Chem. Soc. **128**, 730 (2006).
[10] A. I. Norman, W. H. Zhang, K. L. Beers, and E. J. Amis, J. Colloid Interface Sci. **299**, 580 (2006).
[11] R. Barrett *et al.*, Lab Chip **6**, 494 (2006).
[12] R. G. W. Brown and A. P. Jackson, J. Phys. E **20**, 1503 (1987).
[13] H. S. Dhadwal and B. Chu, Rev. Sci. Instrum. **60**, 845 (1989).
[14] J. P. McClymer, Rev. Sci. Instrum. **61**, 2001 (1990).
[15] R. G. W. Brown, Appl. Opt. **26**, 4846 (1987).
[16] J. Ricka, Appl. Opt. **32**, 2860 (1993).
[17] S. U. Egelhaaf and P. Schurtenberger, Rev. Sci. Instrum. **67**, 540 (1996).
[18] R. G. W. Brown, Appl. Opt. **40**, 4004 (2001).
[19] Equipment and instruments or materials are identified in the paper in order to adequately specify the experimental details. Such identification does not imply recommendation by NIST, nor does it imply the materials are necessarily the best available for the purpose.
[20] G. B. Bantchev, P. S. Russo, R. L. McCarley, and R. P. Hammer, Rev. Sci. Instrum. **77**, 043902 (2006).
[21] H. R. Haller, C. Destor, and D. S. Cannell, Rev. Sci. Instrum. **54**, 973 (1983).
[22] J. O. Hirschfelder, C. F. Curtiss, and R. B. Bird, *Molecular Theory of Gases and Liquids* (Wiley, New York, 1954).
[23] P. Alexandridis and T. A. Hatton, Colloids Surf., A **96**, 1 (1995).
[24] K. Mortensen, Europhys. Lett. **19**, 599 (1992).
[25] The standard uncertainty of all the described DLS measurements is 5%.